Solution Structure of Dimeric Mnt Repressor (1−76)[†,‡]

Maurits J. M. Burgering,[§] Rolf Boelens,[*,§] Dara E. Gilbert,[§,||] Jan N. Breg,[§] Kendall L. Knight,[⊥,#] Robert T. Sauer,[⊥] and Robert Kaptein[§]

Bijvoet Center for Biomolecular Research, Padualaan 8, Utrecht University, 3584 CH Utrecht, The Netherlands, and Department of Biology, Massachusetts Institute of Technology, Cambridge, Massachusetts 023139

Received May 20, 1994; Revised Manuscript Received August 30, 1994[⊗]

ABSTRACT: Wild-type Mnt repressor of *Salmonella* bacteriophage P22 is a tetrameric protein of 82 residues per monomer. A C-terminal deletion mutant of the repressor denoted Mnt (1−76) is a dimer in solution. The structure of this dimer has been determined using NMR. The NMR assignments of the majority of the ^{1}H, ^{15}N, and ^{13}C resonances were obtained using 2D and triple-resonance 3D techniques. Elements of secondary structure were identified on the basis of characteristic sequential and medium range NOEs. For the structure determination more than 1000 NOEs per monomer were obtained, and structures were generated using distance geometry and restrained simulated annealing calculations. The discrimination of intra- vs intermonomer NOEs was based upon the observation of intersubunit NOEs in [^{15}N,^{13}C] double half-filtered NOESY experiments. The N-terminal part of Mnt (residues 1−44), which shows a 40% sequence homology with the Arc repressor, has a similar secondary and tertiary structure. Mnt (1−76) continues with a loop region of irregular structure, a third α-helix, and a random coil C-terminal peptide. Analysis of the secondary structure NOEs, the exchange rates, and the backbone chemical shifts suggests that the carboxy-terminal third helix is less stable than the remainder of the protein, but the observation of intersubunit NOEs for this part of the protein enables the positioning of this helix. The rsmd's between the backbone atoms of the N-terminal part of the Mnt repressor (residues 5−43, 5′−43′) and the Arc repressor is 1.58 Å, and between this region and the corresponding part of the MetJ repressor 1.43 Å.

The Mnt repressor (Vershon et al., 1987) and the closely related Arc repressor of *Salmonella* bacteriophage P22 regulate the expression of the phage *ant* gene [for a review, see Susskind and Youderian (1983)]. Together with the cro and repressor proteins of the phage these proteins control the switch between the lytic and lysogenic state. While the P22 cro and P22 repressors are examples of helix−turn−helix proteins, in which a recognition helix binds specifically into the major groove of DNA, the Arc and Mnt repressors use a β-sheet motif to bind to DNA (Knight et al., 1989; Breg et al., 1990).

The Arc and Mnt repressors together with the MetJ repressor belong to the same family of β-sheet DNA binding proteins (Phillips, 1991). The crystal structure of the MetJ repressor (Rafferty et al., 1989) and the solution structure of the Arc repressor (Breg et al., 1990) have been reported. Cocrystals of the MetJ repressor DNA complex have shown that an N-terminal β-sheet with strands from both monomers of the MetJ dimer binds specifically into the major groove of DNA (Somers & Phillips, 1992). A similar situation is observed in the crystal structure of the Arc repressor−operator complex (Raumann et al., 1994). Both the Arc and MetJ repressors bind to their operators as tetramers, in which two dimers bind in successive major grooves of the DNA and interact via protein−protein contacts.

For Mnt repressor, however, no structural information is available, although the protein is biochemically and genetically well characterized (Vershon et al., 1985; Knight et al., 1989). Mnt repressor is a tetramer (82 residues/monomer) and its N-terminal part is 40% homologous to the dimeric Arc repressor (53 residues/monomer). Mutational analysis of the N-terminal region of the Mnt repressor has identified residues that are functionally important in DNA binding (Youderian et al., 1983; Knight & Sauer, 1989a,b). These studies show that in particular the side chains of Arg^{2}, His^{6}, Asn^{8}, and Arg^{10} are critical for high-affinity binding to operator DNA. A set of C-terminal deletion mutants of the Mnt repressor has been constructed that indicate that determinants for tetramer formation are located in the six carboxy-terminal residues (Knight & Sauer, 1988). Thus, a truncated repressor, in which the six C-terminal residues of wild-type Mnt have been removed, is a dimer in solution which still binds sequence specifically to the *mnt* operator (Knight & Sauer, 1988). However, the affinity is reduced with respect to wild-type Mnt repressor, which may be due to the disruption of the interface region responsible for tetramer formation. The importance of individual base pairs in the *mnt* operator has been probed by protection and interference experiments and mutagenesis studies (Knight & Sauer, 1992).

[†] This work was supported by The Netherlands Foundation for Biophysics and The Netherlands Organization for Chemical Research (SON) with financial aid from The Netherlands Organization for the Advancement of Research (NWO). D.E.G. was supported by USPHS postdoctoral fellowship Grant GM14548.

[‡] Protein coordinates have been submitted to the Brookhaven Protein Data Bank under file name 1MNT.

* Corresponding author. Telephone: 31 30 532184. Fax: 31 30 540980.

[§] Utrecht University.

[||] Present address: Department of Biological Chemistry and Molecular Pharmacology, Harvard Medical School, 240 Longwood Ave., Boston, MA 02115.

[⊥] Massachusetts Institute of Technology.

[#] Present address: Department of Biochemistry, University of Massachusetts, Medical Centre, 55 Lake Ave., Worcester, MA 01655.

[⊗] Abstract published in *Advance ACS Abstracts,* October 15, 1994.

0006-2960/94/0433-15036$04.50/0

In the present paper we report the NMR assignments and three-dimensional structure of Mnt (1−76). Although it is not surprising that the N-terminal part of the Mnt repressor is similar to that of the Arc and MetJ repressors, it is interesting to note that the structural homology is slightly larger with the MetJ repressor than with the Arc repressor. In addition a third α-helix is identified in the C-terminal region which is in dynamic equilibrium with an unfolded structure.

MATERIALS AND METHODS

Sample Preparation. The dimeric Mnt (1−76) mutant was obtained from *Escherichia coli* X90 (Arg^-) strain containing plasmid *Lamb77*, as described (Vershon et al., 1985; Knight & Sauer, 1988) and was extensively dialyzed and then lyophilized. The protein was dissolved in either D_2O or H_2O, the latter containing 5% (v/v) D_2O for the deuterium lock, to a concentration of 2.0−4.0 mM (monomer), and the pH was adjusted to 4.2−4.5. The ionic strength in combination with the pH has a large influence on the solubility of the protein at this concentration. The protein was lyophilized between measuring in H_2O and D_2O.

^{15}N-labeled as well as ^{15}N-,^{13}C-labeled Mnt (1−76) was prepared by first adapting the *E. coli* strain to S. V. medium [phosphate buffer at pH 7.0, ammonium chloride, traces of magnesium sulfate and Mohrs salt, thiamine, ampicilline and glucose (0.2−1.0%)]. The protein yield was not notably affected by these conditions. The sole nitrogen source of this medium was $^{15}NH_4Cl$ (Isotec Inc.); the carbon source was either unlabeled or uniformly ^{13}C-labeled glucose (Isotec Inc.).

NMR Spectroscopy. All NMR spectra were recorded on Bruker AMX500 or Bruker AMX600 spectrometers at 27−30 °C. The spectra were processed on μVAX or on Silicon Graphics computers with NMR processing software (TRITON) developed in our laboratory. All homonuclear 2D spectra were recorded in the pure-phase absorption mode by application of TPPI[1] and with a proton spectral width of 10.5 ppm. The water signal was suppressed by irradiation in the recycle delay and during the mixing time of the NOESY experiments. HOHAHA or (clean-)TOCSY (Bax & Davis, 1985; Griesinger et al., 1988) spectra were recorded with mixing times of 17.5, 34.4, and 60 ms, NOESY (Jeener et al., 1982) spectra with mixing times of 50, 100, 150, and 200 ms, respectively. The 2D datasets of 512 × 2048 points (ω_1, ω_2), obtained both in H_2O and D_2O, were processed with a sine-bell window shifted over $\pi/4$ in both directions and after the double Fourier transformation, baseline corrected to obtain a 1024 × 1024 points spectral data matrix.

The following double resonance [^1H,^{15}N] 3D spectra were acquired: NOESY-HMQC (Zuiderweg & Fesik, 1989; Marion et al., 1989), HMQC-NOESY-HMQC (Ikura et al., 1990a; Frenkiel et al., 1990), and HOHAHA-HMQC (Marion et al., 1989). The NOESY experiments were recorded with a mixing time of 100 ms and the HOHAHA experiment with a mixing time of 26.2 ms. Slowly exchanging amide protons were studied by collecting a 2D [^1H,^{15}N]HMQC spectrum (recording time 30 min) of protonated ^{15}N-labeled Mnt (1−76) 4 min after dissolving it in D_2O. These heterocorrelation experiments were recorded with the ^{15}N carrier in the center of the amide region with a ^{15}N spectral width of 50 ppm. In these [^1H,^{15}N] experiments the heteronuclear *J*-coupling refocusing delay was set to 4 ms.

A set of four triple resonance [^1H,^{15}N,^{13}C] 3D experiments was recorded: HNCA, HNCO (Ikura et al., 1990b; Kay et al., 1990), HN(CO)CA (Bax & Ikura, 1991), and HCANNH (Kay et al., 1991), to make backbone sequential assignments. To obtain assignments of side chain carbon resonances, the double-resonance 3D [^1H,^{13}C]HCCH-TOCSY (Clore et al., 1990) and HMQC-NOESY (Ikura et al., 1990c; Zuiderweg et al., 1990) experiments were recorded. The double- and triple-resonance NMR spectra were directly analyzed on a Silicon Graphics workstation using ALISON (Kleywegt et al., 1993).

Structure Calculation. Protein structures were generated with distance geometry (Havel, 1991) from NOE restraint data using the DGII program (Biosym, San-Diego). The distance geometry procedure consisted of three steps: triangulation, embedding in three dimensions, and an optimization step for both distances and chiralities (250 steps using a conjugate gradient optimization). The protein structures were further refined with restrained simulated annealing using a consistent valence force-field with the program Discover (Biosym, San-Diego). Displaying and visual inspection of structures were performed on Silicon Graphics workstations using the InsightII program (Biosym, San-Diego).

RESULTS AND DISCUSSION

Spin System Analysis. The NMR spectra of Mnt (1−76) repressor indicate that the dimer is symmetric. Assignments of proton resonances started by tracing the spin systems of alanines, valines, threonines, and AMX systems in the homonuclear 2D spectra. In the HOHAHA spectra of Mnt (1−76) in D_2O several AMX spin systems, five out of seven alanines, the two threonines, and all five valines with equal intensity cross-peaks for the methyl protons at H_β and relay cross-peaks at H_α positions, were found. The methyl protons of three out of five leucines were recognized due to a favorable dispersion of the chemical shifts. The single isoleucine was assigned by a relay H_α-methyl cross-peak in a HOHAHA spectrum with a long mixing time. Furthermore, the connectivities of all aromatic ring protons was straightforward and the connectivity to the H_α and H_β resonances of the aromatic residues was established using NOEs with the corresponding aromatic protons.

Sequence Specific Assignment. The 600-MHz NOESY spectrum in H_2O of Mnt (1−76) was used as a start for the sequential analysis using strategies described by Wüthrich (1986) and Englander and Wand (1987). A stretch of six residues between Pro^5 and Pro^{12} was sequentially assigned starting at the unique His^6 spin system. Several strong sequential $d_{\alpha N}(i,i+1)$ NOEs were found, and residues Phe^7 through Met^{11} could be assigned. The NOESY spectrum in H_2O revealed a large number of sequential d_{NN} contacts which led to the recognition of short stretches of adjacent residues. The identification of a limited number of side chains was used to position these stretches within the

[1] Abbreviations: 2D, two dimensional; 3D, three dimensional; HOHAHA, homonuclear Hartmann−Hahn spectroscopy; HMQC, heteronuclear multiple-quantum correlation spectroscopy; NOE, nuclear Overhauser effect; NOESY, 2D NOE spectroscopy; TPPI, time-proportional phase increment.

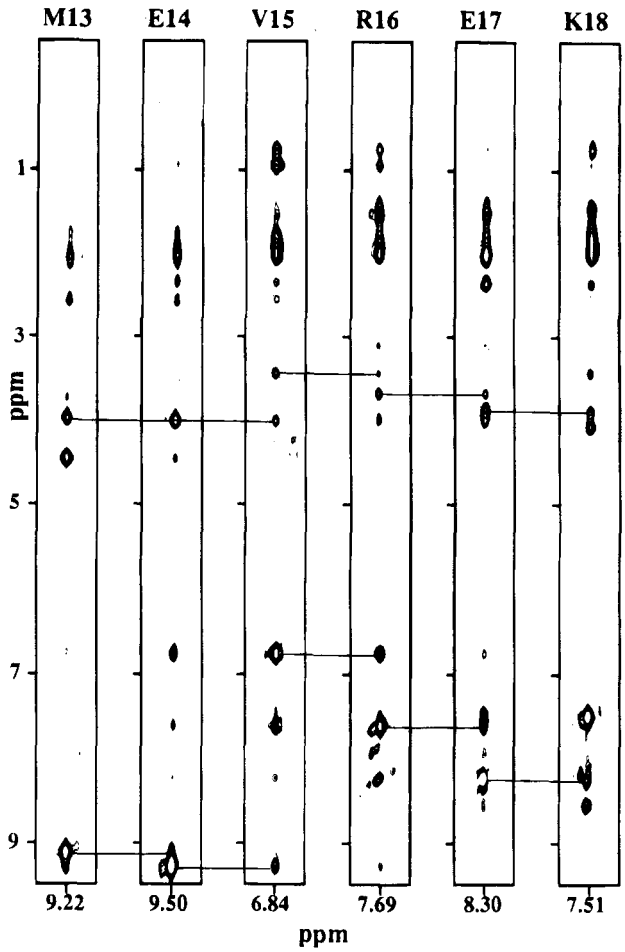

FIGURE 1: Strips of a 600-MHz 3D [^{1}H,^{15}N]NOESY-HMQC spectrum showing sequential d_{NN} NOEs and $d_{\alpha N}$ NOEs of residues 13−18 connected by horizontal bars.

sequence of Mnt (1−76). For instance, the spin system of a valine and a phenylalanine residue within a long stretch of d_{NN} NOEs could be identified as Val^{15} and Phe^{21}. A pair of methyl proton resonances of a leucine was sequentially assigned to Leu^{19}. This stretch of d_{NN} NOEs yielded the assignments for the residues 13−23. Another valine (Val^{38}) was also part of a stretch of d_{NN} NOEs which included the spin systems, Asp^{40}, Ala^{41}, and Ile^{37}. Furthermore, the methyl proton resonances of two leucines, 34 and 35, were found as part of this stretch. Using this long sequence of sequential d_{NN} NOEs, the assignments of the residues from Met^{30} to Lys^{44} were deduced.

Since the C-terminal residues could not be completely assigned at this stage, we made use of heteronuclear [^{1}H,^{15}N] 3D spectra. In the 3D NOESY-HMQC all the previously made sequential assignments were easily confirmed and extended in the ^{15}N planes of the spectrum as shown in Figure 1. The sequential d_{NN} NOEs of degenerate or nearly degenerate sequential amides, which could hardly be observed in both the homonuclear 2D or the heteronuclear 3D NOESY-HMQC spectra, were observed in the 3D [^{1}H,^{15}N]-HMQC-NOESY-HMQC spectrum (Figure 2). This was especially helpful for making assignments in the C-terminal part of the protein where considerable resonance overlap occurs.

All sequential assignments were confirmed by 3D [^{1}H,^{15}N,^{13}C] triple-resonance experiments. Individual amide proton and nitrogen frequencies were connected to the intra

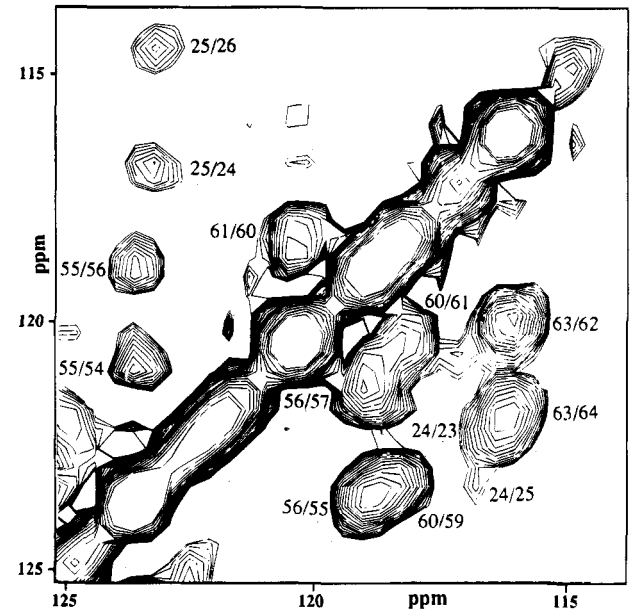

FIGURE 2: ω3 plane at 8.14 ppm in the 3D [^{1}H,^{15}N]HMQC-NOE-HMQC spectrum. The d_{NN} NOEs observed are indicated by numbers. Three examples (24/25, 55/56, and 60/61) of d_{NN} NOEs with degenerate or nearly degenerate amide proton chemical shifts are indicated in this plane.

and preceding $^{13}C_\alpha$ frequencies using the HNCA and HN-(CO)CA spectra. Together with the HNCO spectrum, this permitted the determination of the $C_\alpha(i)$, $C_\alpha(i-1)$, and the $CO(i-1)$ frequencies of essentially all backbone atoms. The H_α frequencies of the amide groups were cross-checked in the HCANNH spectrum allowing a consistent assignment of all backbone frequencies. Analysis of the [^{1}H,^{13}C]HCCH-TOCSY and [^{1}H,^{13}C]HMQC-NOESY spectra provided the assignment of side chain carbon frequencies. The assignments that have been obtained so far are compiled in Table 1.

Short and medium range NOEs. Figure 3 shows the sequence of the Mnt repressor (1−76) and a overview of short- and medium-range NOEs found in both the 2D homonuclear and the 3D heteronuclear NOESY NMR experiments and the presence of slowly exchanging amide protons. The first three N-terminal residues in Mnt (1−76) appear to be flexibly disordered in solution since these spin systems give strong HOHAHA cross-peaks whereas the NOESY cross-peaks are considerably weaker. Strong sequential $d_{\alpha N}(i,i+1)$ NOEs are indicative of a more or less extended structure. For the segment Pro^5−Pro^{12} strong sequential $d_{\alpha N}(i,i+1)$ and weak or absent d_{NN} NOEs are present. The strong NOE between the α-protons of His^6 and Arg^{10} and the medium intensity $d_{\alpha N}$ NOEs between residues 10−7 and 6−11 and between the amide protons of residues 7 and 9 indicate that this region of the Mnt repressor consists of a intersubunit β-sheet similar to the Arc repressor (Breg et al., 1989).

Residue Pro^{12} has an strong sequential $d_{\alpha N}$ NOE to Met^{13}. A stretch of strong d_{NN} NOEs in conjunction with weaker $d_{\alpha N}(i,i+1)$ NOEs is observed from residue 13 through 26. An α-helix is present in this region as judged from the medium range $d_{\alpha N}(i,i+3)$, $d_{\alpha N}(i,i+4)$, and $d_{\alpha\beta}(i,i+3)$ NOEs and the presence of slowly exchanging amides.

A turn region between residues Asn^{26} and Ser^{29} which has a completely conserved homology with Arc is characterized

Table 1: ^{1}H, ^{15}N, and ^{13}C Chemical Shifts and Assignments of Mnt 1−76[a]

residue	^{15}N	NH	$^{13}C\alpha$	Hα	^{13}CO	$^{13}C\beta$	Hβ	others[b]
Ala[1]			49.68	4.13	171.9	17.43	1.56	
Arg[2]	121.2	8.71	54.74	4.30	173.7	28.48	1.78	γ 24.86 (1.64), δ 41.26 (3.25), ϵ 84.4 (7.31)
Asp[3]	121.4	8.42	51.47	4.65	173.3	38.58	2.63	
Asp[4]	123.0	8.09	50.53	4.84		31.74	2.78/2.41	
Pro[5]			61.03	4.49	173.5		2.22	γ 25.20 (1.97), δ 48.60 (3.76/4.00)
His[6]	116.9	8.34	52.64	5.21	171.7	28.28	3.01/3.09	ζ 134.85 (8.60), δ 130.74 (7.11)
Phe[7]	123.8	9.07	55.42	4.64	171.0		2.89/2.96	δ 127.20 (7.15), ϵ 127.20 (7.45), ζ 127.68 (7.27)
Asn[8]	127.4	8.19	50.58	4.98	171.0	35.91	2.50/2.61	δ 111.20 (7.31/6.53)
Phe[9]	127.6	8.82	52.55	5.22	171.8	28.80	3.27/3.58	δ 127.10 (7.35), ϵ 127.10 (7.15), ζ (124.14) 6.81
Arg[10]	130.4	9.30	53.44	4.44	172.4	29.74	1.54/1.72	γ 25.24 (1.31), δ (3.12), ϵ 84.4 (7.35)
Met[11]	123.4	8.01	54.84	4.61		28.00	1.28/2.58	γ (3.07), ϵ 15.76 (1.41), γ (3.18), δ (3.82)
Pro[12]			60.19	4.52	175.9			
Met[13]	125.6	9.22	56.86	4.03	175.6	29.77	2.62/2.58	γ (2.23/2.18), ϵ 14.60 (2.07)
Glu[14]	117.5	9.50	57.56	4.08	176.9	26.34	1.89/2.07	γ 33.32 (2.35)
Val[15]	119.0	6.84	63.58	3.50	174.3	29.41	1.93	γ_1 19.18 (0.90),[c] γ_2 20.89 (0.81)
Arg[16]	121.5	7.69	58.38	3.73	176.3			γ (1.43/1.51), δ (3.16), ϵ 84.0 (7.52)
Glu[17]	117.1	8.30	56.96	3.94	176.5	26.53	2.08	γ (2.37)
Lys[18]	119.6	7.51	57.81	4.13	177.7	31.45	1.95	γ 27.09 (1.79), δ 27.09 (1.63), ϵ 40.00 (2.95)
Leu[19]	122.5	8.60	55.91	3.95	175.3	39.55	1.85	γ 25.18 (1.51), δ 23.51 (0.68), δ' 21.55 (0.80)
Lys[20]	121.1	8.39	57.94	3.84	176.5		1.49	γ 22.38 (1.22), δ 27.34 (1.56/1.67), ϵ 39.82 (2.87)
Phe[21]	118.6	7.96	58.83	4.36	176.2	36.51	3.17/3.25	δ (7.32), ϵ (7.36)
Arg[22]	121.6	8.08	56.68	4.03	175.4		1.49	γ (1.65), δ (2.95/3.25), ϵ 84.1 (7.89)
Ala[23]	122.5	8.56	53.50	4.05	177.7	15.56	1.38	
Glu[24]	117.1	8.14	57.03	4.03	178.5		1.98/2.14	γ (2.37/2.59)
Ala[25]	123.3	8.15	52.79	4.07	176.8	15.56	1.38	
Asn[26]	114.6	7.73	50.62	4.83	173.3	38.75	2.79	δ 113.9 (6.68/8.30)
Gly[27]	110.8	8.00	44.87	3.94	172.4			
Arg[28]	118.2	8.33	52.23	4.88	173.1		1.85	γ (1.64/1.57), δ (3.00/3.25), ϵ 84.6 (7.62)
Ser[29]	115.3	8.49	55.15	4.52	173.3		4.11	
Met[30]	121.7	9.27	58.54	3.74	175.7	31.06	1.86/2.12	γ 31.09 (2.47), ϵ 14.42 (1.71)
Asn[31]	117.3	8.89	56.47	4.45	175.0	38.50	3.05	δ 113.9 (7.87/7.89)
Ser[32]	115.1	8.22	57.52	4.33	174.8	61.48	4.13/4.01	
Glu[33]	124.3	8.71	56.88	3.94	175.3		1.92	γ (2.11)
Leu[34]	119.6	8.29	55.66	3.86	175.9	39.30	1.35	γ 24.52 (0.91), δ 22.40 (0.46), δ' 23.63 (0.21)
Leu[35]	118.7	8.53	56.36	4.22	176.2		2.03	γ 24.85 (1.88), δ 22.18 (1.06), δ' 22.18 (1.02)
Gln[36]	120.0	7.95	56.99	3.92	176.0	25.43	2.15/2.20	γ 21.32 (2.36), ϵ 114.7 (7.71/6.76)
Ile[37]	119.9	8.14	63.32	3.76	177.5	36.49	1.98	γ 12.01 (0.77), δ 15.39 (0.77)
Val[38]	121.0	8.54	65.10	3.57	175.0	29.70	2.22	γ_1 20.16 (0.92), γ_2 22.17 (0.96)
Gln[39]	120.1	9.01	57.94	3.98	177.5	26.49	2.09/2.23	γ 21.32 (2.23/2.53), ϵ 110.3 (7.07/6.69)
Asp[40]	120.0	8.55	55.21	4.38	176.6	37.72	2.83/2.65	
Ala[41]	122.6	7.76	52.89	4.22	178.4	17.20	1.57	
Leu[42]	115.8	8.27	53.71	4.23	175.6		2.05/2.02	γ (1.89), δ (0.77), δ' (0.83)
Ser[43]	114.6	7.65	57.23	4.43	171.5	61.90	4.04	
Lys[44]	123.7	7.49	51.92	4.68		30.74	1.89	γ 22.26 (1.48), δ 27.30 (1.68), ϵ 40.00 (2.99)
Pro[45]			60.84	4.45	174.9	29.92	1.86/2.29	γ 25.09 (2.00), δ 48.45 (3.62/3.85)
Ser[46]	118.8	8.53	54.38	4.72		60.84	3.83/3.88	
Pro[47]			61.23	4.49	174.9	29.96	1.93/2.29	γ 25.24 (2.00), δ 48.45 (3.82/3.74)
Val[48]	120.6	8.18	60.48	4.16	174.5	30.41	2.09	γ 18.32 (0.95)
Thr[49]	117.5	8.12	59.79	4.34	172.7	67.85	4.18	γ 19.29 (1.18)
Gly[50]	111.2	8.25	43.13	3.93	171.4			
Tyr[51]	120.6	8.04	55.92	4.55	173.7	36.90	2.94/3.02	δ 116.1 (6.84) ϵ 117.6 (7.09)
Arg[52]	123.6	8.30	54.00	4.28	173.5		1.70/1.81	γ (1.58), δ (3.08), ϵ 84.4 (7.41)
Asn[53]	119.6	8.28	50.90	4.67	173.0	36.71	2.89	δ 112.9 (7.58/6.91)
Asp[54]	121.3	8.42	53.17	4.53	174.2	38.58	2.71	
Ala[55]	123.6	8.18	51.76	4.16	177.0	16.44	1.42	
Glu[56]	119.1	8.18	55.25	4.13	174.9	27.08	2.08	γ (2.34/2.42)
Arg[57]	121.6	7.98	55.31	4.06	174.6	28.16	1.72/1.88	δ (1.60/1.53), δ (3.08), ϵ 84.2 (7.34)
Leu[58]	121.7	8.11	54.20	4.21	174.6		2.54	δ (0.86), δ' (0.89)
Ala[59]	123.4	8.05	51.53	4.17	176.6	16.48	1.44	
Asp[60]	118.5	8.14	52.76	4.60	174.9	38.01	2.81	
Glu[61]	120.2	8.24	55.03	4.24	174.5			γ 2.47
Gln[62]	120.8	8.27	53.82	4.23	173.8		2.18	γ (2.43), ϵ 112.5 (7.46/6.80)
Ser[63]	116.1	8.16	56.46	4.35	173.0	61.29	3.93/4.00	
Glu[64]	121.8	8.18	55.14	4.24	174.8		2.12	γ (2.39)
Leu[65]	121.8	7.95	54.30	4.22	176.0	40.16	1.63	γ 24.80 (1.63), δ 22.77 (0.90), δ' 22.45 (0.95)
Val[66]	119.9	7.79	61.39	3.97	176.0	30.17	2.14	γ_1 18.96 (1.00), γ_2 18.96 (0.94)
Lys[67]	123.9	8.03	55.05	4.17	174.6	33.36	1.37	γ 28.44 (1.69/1.60), ϵ 40.10 (2.98)
Lys[68]	121.2	8.07	54.71	4.24	174.4			
Met[69]	121.7	8.18	53.83	4.40	174.0		2.00	γ (2.57/2.49)
Val[70]	121.2	7.94	60.50	4.03	173.7	30.63	2.00	γ_1 19.27 (0.82), γ_2 18.49 (0.87)
Phe[71]	123.6	8.22	55.75	4.65	173.3		3.01/3.21	δ (7.27), ϵ (7.31)
Asp[72]	121.5	8.33	52.04	4.66	173.9		2.68/2.77	
Thr[73]	114.7	8.05	60.05	4.28	172.9	67.87	4.28	γ 19.50 (1.23)
Leu[74]	124.5	8.15	53.27	4.34	175.0		1.61/1.67	γ (1.38), δ (0.83)
Lys[75]	122.2	8.15	53.99	4.32	173.3	30.85	1.84	γ 22.32 (1.45), δ 26.91 (1.74), ϵ 40.08 (3.02)
Asp[76]	125.4	7.97	52.50	4.49		30.85	2.70/2.77	

[a] ^{1}H Chemical shifts are reported in ppm with an accuracy of ±0.02 ppm relative to the H_2O or HDO signal, which resonates at 4.75 ppm. ^{15}N Chemical shifts are reported in ppm with an accuracy of ±0.1 ppm relative to the $^{15}NH_4Cl$ (acidic) signal, which resonates at 22.3 ppm. ^{13}C Chemical shifts are reported in ppm with an accuracy of ±0.1 ppm relative to the ^{13}C methyl signal of TMS, which resonates at 0 ppm. [b] Chemical shifts of the heteronucleus first, between brackets the proton chemical shifts. [b] Valine methyls are stereospecifically assigned as γ_1/γ_2 according to the IUPAC-IUB conventions (IUPAC-IUB Commission on Biochemical Nomenclature).

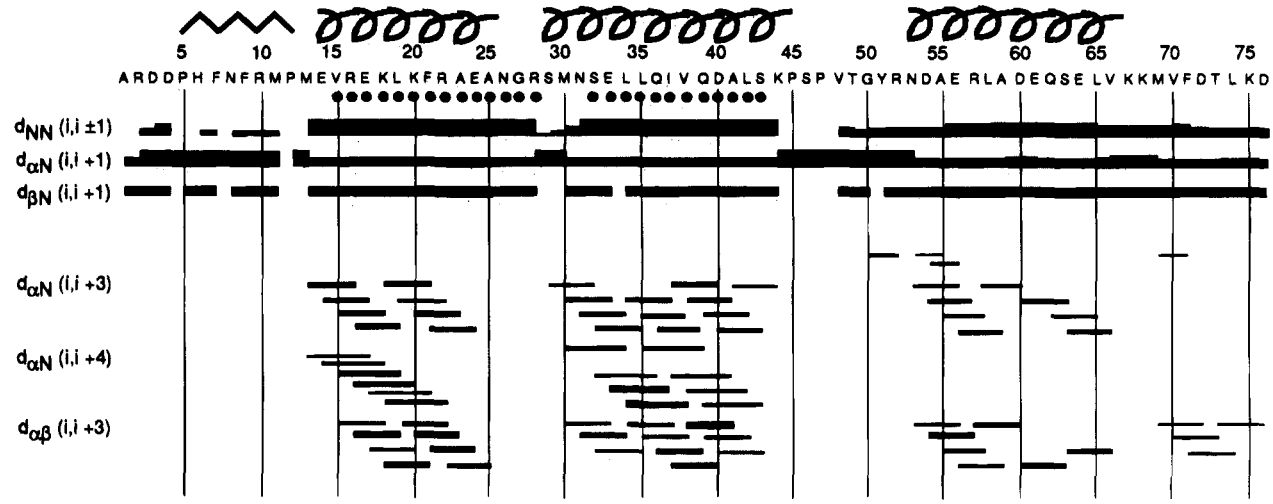

FIGURE 3: Amino acid sequence of Mnt (1−76) repressor together with a schematic summary of short- and medium-range NOEs observed indicating regions of secondary structure. The thickness of the connecting bars is a measure for the intensity of the NOEs. The filled circles under the amino acid sequence denote residues with slowly exchanging amide protons. Sequential $d_{\alpha\delta}(i,i+1)$ NOEs of prolines are indicated at $d_{\alpha N}(i,i+1)$.

by strong sequential $d_{\alpha N}$ NOEs for residues Ala[25] and Arg[28] and a $d_{NN}(i,i+2)$ NOE between the amides of Asn[26] and Arg[28].

The segment Met[30]−Lys[44] is characterized as another α-helix because an uninterrupted stretch of strong d_{NN} NOEs is observed and many medium-range NOEs are present throughout this sequence. At Pro[45] the sequence homology between Arc and Mnt (1−76) stops. Relatively strong $d_{\alpha N}(i,i+1)$ and weaker d_{NN} NOEs are found in the region Pro[45] through Asn[53], although for residues 49 and 50 the latter are stronger. This region is also characterized by several intermonomer medium-range NOEs such as from the H_β protons of Ser[46] to the amide of Val[48] and the H_α protons of Gly[50] to the amide of Arg[52]. Furthermore NOEs of the amide of Asp[54] with the H_α and H_β methyl protons of Ala[55] are present.

Starting with $d_{\alpha N}(i,i+3)$ and $d_{\alpha N}(i,i+2)$ NOEs of Asn[53] and Asp[54] (the latter being weak), several $d_{\alpha N}(i,i+3)$, $d_{\alpha\beta}(i,i+3)$, and stronger d_{NN} NOEs indicate the presence of a third α-helix in the sequence of Mnt (1−76). Not all α-helical medium-range NOEs are found for this region, and in contrast to the first two helices of Mnt (1−76) slowly exchanging amides were not present, indicating that the third helix is in dynamic equilibrium with a unfolded structure. The C-terminal residues Met[67]−Asp[76] have no clear characteristic sequential or medium-range NOEs to indicate a well defined regular secondary structure.

Chemical Shift Analysis. Chemical shifts are useful indicators of the secondary structure as described by Wishart et al. (1991). H_α protons have lower frequencies in α-helixes and higher frequencies in β-sheet compared to random coil, and the $^{13}C_\alpha$ and ^{13}CO shifts show a similar variation, except with an opposite sign. Figure 4 shows plots of the backbone chemical shift deviations with respect to random coil values for the residues along the sequence of Mnt (1−76) and an unweighted linear combination of the H_α, $^{13}C_\alpha$, and ^{13}CO chemical shifts. In these plots the correspondence between the chemical shift and the secondary structure, indicated in the combination plot, is remarkable for the β-sheet and the first two α-helices. However, the backbone chemical shifts of residues in third α-helix are almost invariable close to random coil values. Residues in helices or β-strands that are in equilibrium with random coil structure are expected to have backbone chemical shifts closer to random coil values, while the shifts in rigid helices or β-strands deviate more from random coil values.

Solution Structure of the Mnt Repressor (1−76). The structure determination of the Mnt (1−76) was done in two stages. In the first stage we modeled the structure of the part which is homologous to the Arc repressor. Distance geometry and restrained simulated annealing calculation were performed for a dimer consisting of residues 1−44. From 2D NOESY spectra with various mixing times both in H_2O and D_2O, cross-peaks were assigned, integrated-, and translated into distance restraints by determining the initial build-up rates of the NOEs. The tyrosine $H_\delta-H_\epsilon$ cross-peaks were used as a calibration with a distances of 2.45 Å. To all distances an error of 10% and appropriate pseudo-atom corrections were added. These distances were used as upper bounds. The lower bounds of the distance restraints were set to 2 Å. The NOE restraint data were supplemented with hydrogen bonds for the defined secondary structure elements.

For the part of the Mnt dimer homologous with Arc, 1764 distance restraints were obtained derived from 514 intraresidue, 372 sequential, 474 medium-range, and 404 long-range NOEs and 60 restraints for hydrogen bounds. The intramonomeric long-range NOEs (112) were initially distinguished from intermonomer NOEs (292) with the aid of a protein model. This model was obtained with computer graphics model building techniques using InsightII software (Biosym, San-Diego), replacing the amino acid side chains of the solution structure of Arc (Breg et al., 1990) by those of Mnt assuming a structural homology. The intermonomer NOEs thus obtained were confirmed by 2D [^{12}C,^{13}C] and time-shared [^{15}N,^{13}C] double-filtered NOESY experiments on Mnt (1−76) heterodimers consisting of labeled [^{13}C,^{15}N] monomer and unlabeled monomer (Burgering et al., 1993a,b). A family of 20 protein structures was generated with distance geometry from the NOE restraint data and further refined with restraint molecular dynamics and energy minimization. The set of conformers satisfies the distance restraints, an average of 15.9 restraints per monomer were violated by more than 0.6 Å, and 1.4 restraints on average were violated by more than 1.0 Å (cf. Table 2). Figure 5a shows the 20

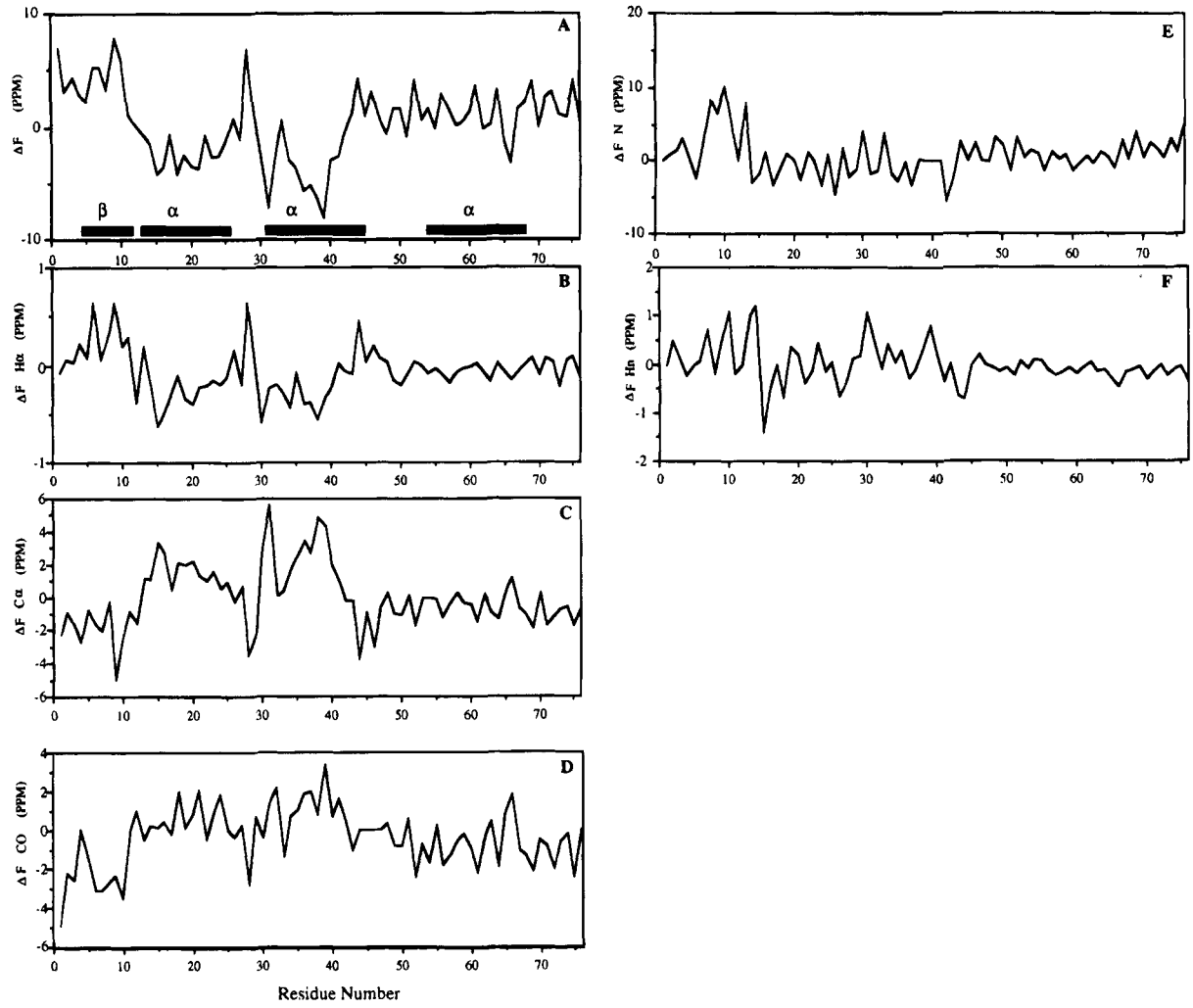

FIGURE 4: Deviations, ΔF, from the random coil shifts for the linear combination (Hα−Cα−CO) of the backbone chemical shifts along the sequence of Mnt (1−76) (panel **A**) with the secondary structure indicated. The individual chemical shift deviations (Hα panel B; Cα panel C; CO panel D) of Mnt (1−76) are presented in the panels below. For completeness also the amide nitrogen (E) and amide proton (F) deviations from random coil chemical shift are given. The average chemical shift values from Wishart et al. (1991) are used as random coil values.

structures superimposed on the average structure. Although the first three N-terminal residues are disordered, the central core is well defined and is composed of two intertwined pairs of helices of the symmetric dimer preceded by an antiparallel β-sheet with strands contributed by both monomers. The average root mean square deviations (rmsd) between the set of 20 conformers and the average structure (residues 4−44 and 4′−44′) for the backbone atoms is 0.59 Å and for all heavy atoms 1.08 Å (cf. Table 2).

In the second stage the complete structure of the Mnt repressor (1−76) was considered. For the region of the Mnt mutant (residues 45−76) where no apparent homology exists with the related Arc and MetJ repressors and no structural data are available, the observation of intermonomeric NOEs in the 2D [^{13}C,^{15}N] double half-filtered NOESY experiments (Burgering et al., 1993a,b) was essential. In these spectra intersubunit NOEs were observed between protons of residues in the C-terminal part the protein, which define the topology of the third helix in the solution structure of Mnt (1−76). There are intermonomer NOEs present between the aromatic protons of Tyr^{51} located in the loop region and one face of the helix (Asp$^{60'}$, Ala$^{59'}$, and Arg$^{57'}$). The starting points of the two C-terminal helices in the dimer are close together due to the intermonomer NOEs observed between Asn^{53} and Ala$^{55'}$, and the helices are positioned relative to the N-terminal part of the protein by NOEs observed between Ala^{41} and Leu$^{58'}$. A total of 2064 distance restraints was determined, derived from 518 intraresidue, 448 sequential, 658 medium-range, and 440 long-range NOEs (320 intermonomer NOEs) and 78 restraints for hydrogen bonds (cf. Table 2). These constraints were obtained from the homonuclear NOESY spectra and the double-resonance [^{1}H,^{15}N] and [^{1}H,^{13}C] 3D HMQC-NOESY spectra, the observed intermonomer NOEs, and hydrogen bonds for the well defined secondary structure elements. It should be noted that although there is evidence for a dynamic equilibrium between a folded and a unfolded third helix as discussed above, the structure calculations were performed for the folded form. Figure 5b shows 15 monomer obtained from the distance geometry and energy minimization calculations of the Mnt (1−76) dimer. The bundle defines a single topology of the overall folding, but the third helix is not very well defined compared to the N-terminal core of the protein. This was expected considering the flexible character of this helix; only a few long-range NOEs are observed for this part of the protein. The average rmsd between the 15 conformers (residues 4−44, 53−66, and 4′−44′, 53′−66′) and the average structure is 1.56 Å for the backbone atoms

Table 2: Statistics of the Structure Determination of Mnt Repressor (1−76)

number of NMR restraints used for the structure determination of Mnt repressor (1−76)[a]	
intraresidue	259
sequential	224
medium range	329
hydrogen bonds	39
long range	220
intrasubunit	60
intersubunit	160
total	1032

		rmsd (Å) between the average and the ensemble of 15 Mnt repressor (1−76) structures	
		backbone	all atoms
Mnt	(4−44, 4′−44′)	0.59	1.08
Mnt	(4−44, 53−66) (4′−44′, 53′−66′)	1.56	2.20

		average restraints violations of the ensemble of 15 Mnt repressor (1−76) structures[a]	
		>0.6 Å	>1.0 Å
Mnt	(1−44)	15.9	1.4
Mnt	(1−76)	17.8	1.7

stereochemical quality of the ensemble of 15 Mnt repressor (1−76) structures[b]		
% res. with ϕ/ψ in most favored regions	69.6	class 2
χ_1 standard deviation	16.2	class 2
hydrogen bond energy standard deviation	0.85	class 2

[a] The numbers are given for one monomer. [b] According to Morris et al. (1992) (PROCHECK).

and for all heavy atoms 2.20 Å. The structures satisfy the large set of distance restraints, while on average of 17.8 restraints per monomer were violated by more that 0.6 Å and 1.7 restraints were violated by more than 1.0 Å (cf. Table 2).

The stereochemical quality of the ensemble of 15 structures was checked with the program PROCHECK (Morris et al., 1992). The results are summarized in Table 2. Taken individually, all structures have good stereochemical qualities, seven having a classification of 2, 2, 2 or better and none exceeding a classification of 3 for any of the criteria. The secondary structure elements assigned according to the program PROCHECK revealed a β-sheet between residues 5 and 14, and three α-helices between residues 13−26, 32−43, and 54−66.

In Figure 6 ribbon diagrams of the structures of Mnt repressor (1−76), Arc repressor, and MetJ repressor are presented. In the structure of Mnt (1−76) the carboxy-terminal helices cover the top of the amino-terminal sheet−helix−helix elements. The side chains of the functionally important residues of the Mnt repressor are all located on the exterior of the dimer, in the disordered N-terminus (Arg^2), and the β-sheet (His^6, Asn^8, and Arg^{10}) and can therefore easily be involved in the interaction of the protein with the operator DNA. Superimposing the sheet−helix−helix elements of the Mnt repressor structure and the refined solution structure of Arc (Bonvin et al., 1994) reveals that the conformations of the backbone of the two related proteins are strikingly similar. The pairwise rmsd between backbone atoms of Mnt repressor (residues 5−43, 5′−43′) and Arc repressor (residues 8−46, 8′−46′) is 1.58 Å. The secondary structure elements of the Mnt and Arc repressors coincide completely including the turn region between the first and the second helix. A small difference is noticed between the two structures, the second helix in the Mnt structure being slightly displaced compared to the second helix of the Arc structure. The structure of the MetJ repressor (Rafferty et al., 1989) has a homologous N-terminal sheet−helix−helix motif. Interestingly, the pairwise rmsd between backbone atoms of Mnt repressor (residues 5−26, 30−43, 5′−26′, 3−43′) and MetJ repressor (residues 22−43, 53−66, 22′−43′, 53′−66′) is 1.43 Å, thus slightly lower than with the Arc repressor in spite of the lower degree of homology. The structure of the MetJ repressor is extended with a loop region and an α-helix in a similar way as the Mnt repressor. However, no amino acid sequence homology could be deduced between the C-terminal parts of Mnt and MetJ, and the arrangement of these secondary structure elements in the three-dimensional structures of both proteins is not related.

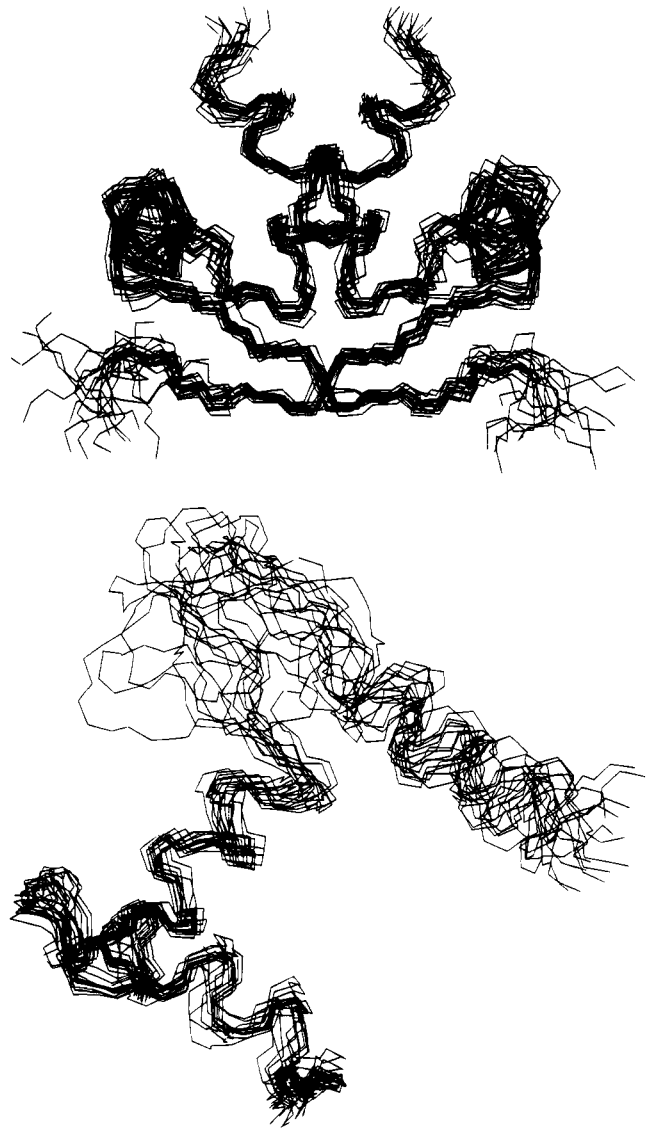

FIGURE 5: (a, top) Backbone traces of 20 conformers of the DNA binding domain of the Mnt (1−76) repressor (residues 1−44, 1′−44′). (b, bottom) Backbone traces of the 15 conformers of the Mnt (1−76) repressor. For display purposes only, the residues 4−66 of one monomer are shown excluding the undefined N- and C-terminal tails. The conformers are 90° rotated along the *y*-axis relative to the orientation of panel a. The view is along the β-sheet.

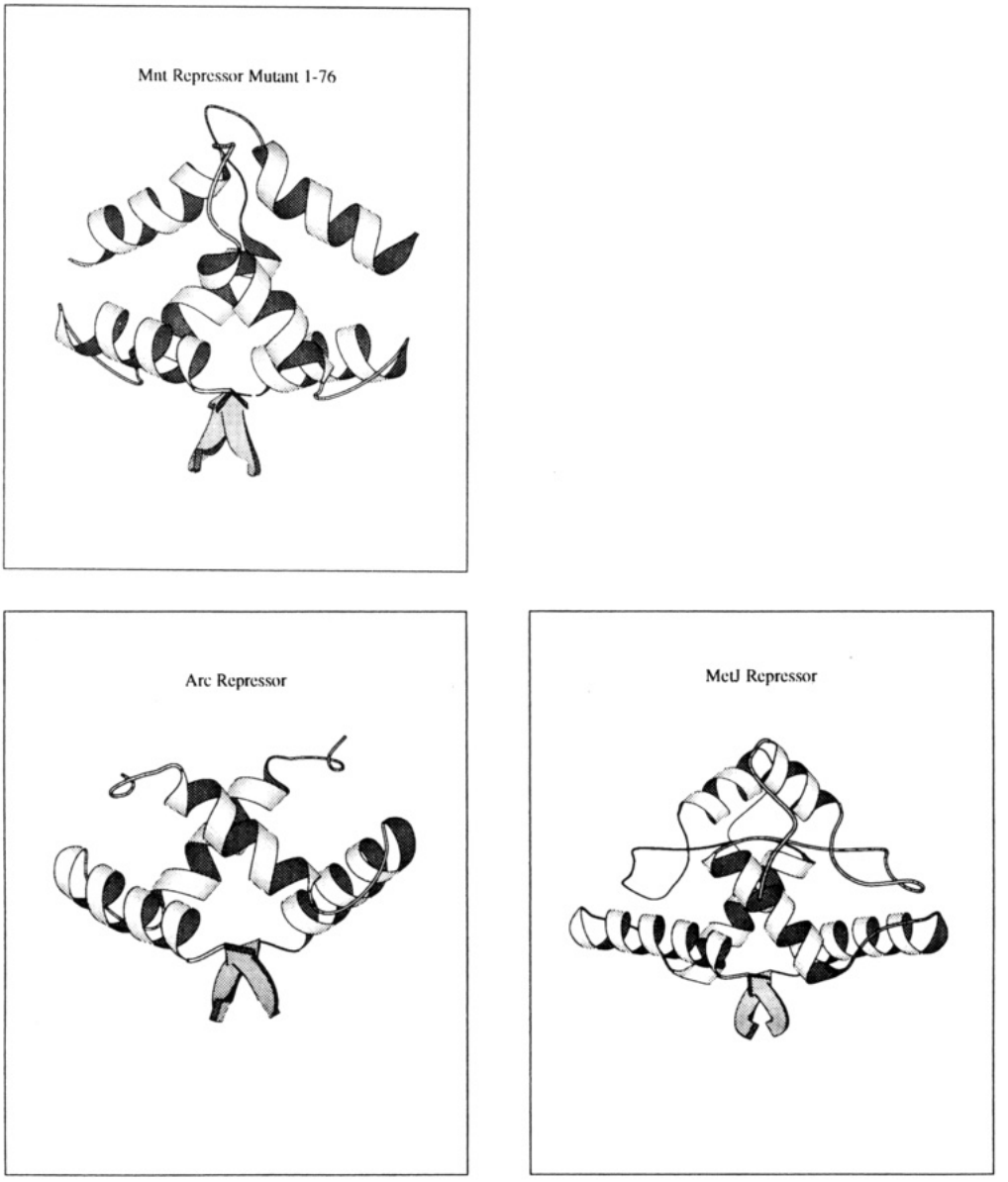

FIGURE 6: Ribbon diagram representing the complete folding of the Mnt (1−76) repressor (residues 4−66, 4′−66′ of each monomer) using the program Molscript (Kraulis, 1991). Also shown are the solution structure of the Arc repressor (Bonvin et al., 1994) and crystal structure of the MetJ repressor (Rafferty et al., 1989). The β-sheets are represented by arrows, the helices by ribbons.

Preliminary Studies on Wild-Type Mnt. The fact that wild-type Mnt repressor is a tetramer in solution raises interesting questions about its symmetry. Crystal structures of symmetric tetramers may have C_4 or D_2 symmetry (Schulz & Schirmer, 1979; Creighton, 1993). If such a symmetry is present for the wild-type Mnt tetramer, the protein would have to undergo a major conformational change to the "dimer of dimers" structure upon DNA binding (assuming the protein−DNA complex is similar to that of the Arc and MetJ repressors). On the other hand, if it is already a dimer of dimers in solution, what would prevent it from further oligomerization? An NMR study of wild-type Mnt repressor could shed light on these questions. The NMR spectra of wild-type Mnt (38 kDa) resemble those of Mnt (1−76) (17.5 kDa), although the line width are broader in accordance with the almost double size of the protein. Many of the assignments of Mnt (1−76) can be directly transferred to the spectra of wild-type Mnt. The chemical shifts of all the resonances of the residues 1−44, i.e., N-terminus, β-sheet, first α-helix, turn, and second α-helix, are almost identical for both proteins. In contrast, for the C-terminal residues an interesting doubling of resonances occurs. In Figure 7 two planes are shown at the nitrogen chemical shift (111 ppm) of Gly^{27} and Gly^{50} from the 3D [^{1}H,^{15}N]NOESY-HMQC spectra of Mnt (1−76) and wild-type Mnt, respectively. The chemical shifts of the two glycines in both spectra are similar, including the NOEs observed at the amide protons. However, in the wild-type spectra the resonances of the amide of Gly^{50} and the observed NOEs at the amide are doubled. This doubling of resonances is not present for the residues 1−44 and was only observed for residues in the C-terminal part. Although for the C-terminus a complete assignment has not yet been made, for all residues that have been identified (residues 48, 49, 50, 51, 55, 59, 78, 79, 80) a doubling was observed. We note that this also includes the additional six C-terminal residues of wild-type Mnt.

The observed doubling of resonances in the C-terminus of the repressor near the tetramerization interface excludes C_4 or D_2 symmetry and may point to C_2 symmetry similar to the DNA-bound dimer of dimers of the MetJ and Arc

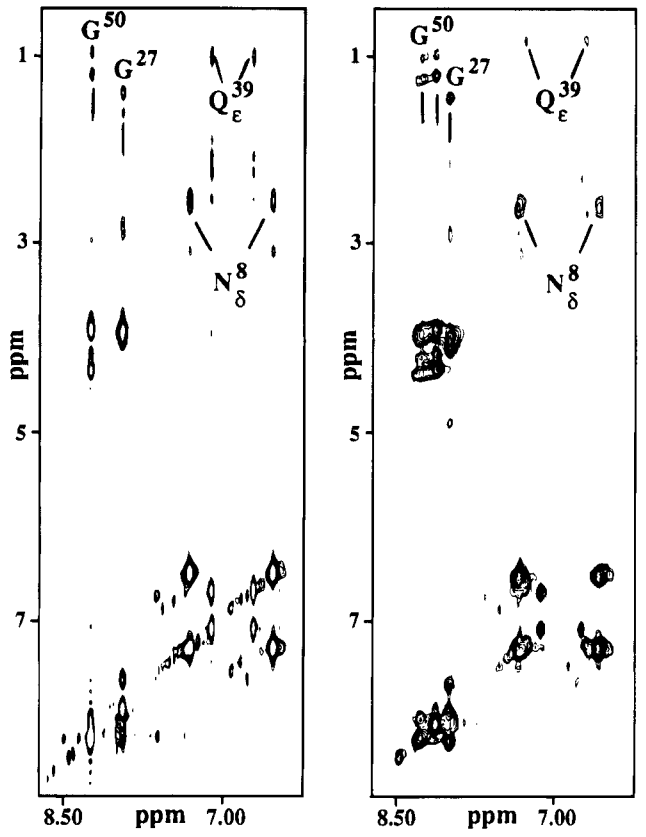

FIGURE 7: Two planes (ω1 ^{1}H, ω3 ^{1}H) from 3D [^{1}H,^{15}N]NOESY-HMQC spectra at the nitrogen chemical shift (111 ppm) of Gly^{27} and Gly^{50} of Mnt (1−76) (left panel) and wild-type Mnt (right panel), respectively. The resonances of Gly^{50} and NOEs observed from the amide of this residue are doubled in the spectrum of wild-type Mnt.

repressors. However, for the free wild-type Mnt repressor contacts between the dimers probably do not involve similar residues as are responsible for tetramerization in the complexes of Arc and MetJ repressors. In the crystal structure of the Arc repressor−operator complex the dimer−dimer contacts are made by the side chains of two Arg^{31} residues, located in the loop between helix one and two (Raumann et al., 1994). The side chains of the arginine residues make hydrogen bonds with the carbonyl of Asn^{29}. In the NMR spectra of wild-type Mnt repressor the resonances of the homologous residues (Arg^{28}, Asn^{26}) are not doubled. This indicates that dimer−dimer contacts are located entirely in the C-terminal region of free Mnt repressor, including not only the six C-terminal residues but also the third helix and the loop between helix two and three. This organization of the tetramer could explain the resonance doubling in the NMR spectra of wild-type Mnt repressor.

It appears that different parts of the Mnt repressor have different functions. The N-terminal sheet−helix−helix is the DNA binding core and forms stable dimers. The C-terminal region, including the third helix, appears to be involved in the tetramer formation. The removal of the C-terminal six residues results in weakening of the tetramer interaction, and Mnt repressor (1−76) becomes dimeric in solution with a destabilized third helix for Mnt (1−76). This helix may only be stable in the full tetrameric structure. The DNA binding specificity is not affected, although a much lower affinity for DNA is now observed probably due to the loss of the favorable tetramer interactions. Thus, similar to many other DNA binding proteins and transcription factors Mnt repressor has two functionally different regions, one involved in the DNA binding and another involved in protein−protein interactions.

ACKNOWLEDGMENT

We thank A. V. E. George for his assistance in the purification of the ^{15}N-labeled protein and D. Schipper (Gist-Brocades B. V., Delft) for recording the 3D [^{1}H,^{15}N]NOESY-HMQC spectrum of Mnt (1−76) and wild-type Mnt.

REFERENCES

Bax, A., & Davis D. G. (1985) *J. Magn. Reson. 65*, 355−360.
Bax, A., & Ikura, M. (1991) *J. Biomol. NMR 1*, 99−104.
Bonvin, A. M. J. J., Vis, H., Breg, J. N., Burgering, M. J. M., Boelens, R., & Kaptein, R. (1994) *J. Mol. Biol. 236*, 586−589.
Breg, J. N., Boelens, R., George, A. V. E., & Kaptein, R. (1989) *Biochemistry 28*, 9826−9833.
Breg, J. N., van Opheusden, J. H. J., Burgering, M. J. M., Boelens, R., & Kaptein, R. (1990) *Nature 346*, 586−589.
Burgering, M. J. M., Boelens, R., Caffrey, M., Breg, J. N., & Kaptein, R. (1993a) *FEBS Lett. 330*, 105−109.
Burgering, M, Boelens, R., & Kaptein, R. (1993b) *J. Biomol. NMR 3*, 709−714.
Clore M. G, Bax, A., Driscoll, P. C., Wingfield, P. T., & Gronenborn, A. M. (1990) *Biochemistry 29*, 8172−8184.
Creighton, T. F. (1993) *Proteins*, second ed., pp 232−236, W. H. Freeman and Company, New York.
Englander, S. W., & Wand, A. J. (1987) *Biochemistry 26*, 5953−5958.
Frenkiel, T., Bauer, C., Carr, M. D., Birdsall, B., & Feeney, J. (1990) *J. Magn. Reson. 90*, 420−425.
Griesinger, C., Otting, G., Wüthrich, K., & Ernst, R. R. (1988 *J. Am. Chem. Soc. 110*, 7870−7872.
Havel, T. F. (1991) *Prog. Biophys. Mol. Biol. 56*, 43−78.
Ikura, M., Bax, A., Clore, M., & Gronenborn, A. (1990a) *J. Am. Chem. Soc. 112*, 9020−9022.
Ikura, M., Kay, L. E., & Bax, A. (1990b) *Biochemistry 29*, 4659−4667.
Ikura, M., Kay, L. E., Tschudin, R., & Bax, A. (1990c) *J. Magn. Reson. 86*, 204−209.
Jeener, J., Meier, B. H., Bachmann, P., & Ernst, R. R. (1982) *J. Chem. Phys. 71*, 4546−4553.
Kay, L. E., Ikura, M., Tschudin, R., & Bax, A. (1990) *J. Magn. Reson. 89*, 496−514.
Kay L. E., Ikura, M., & Bax, A. (1991) *J. Magn. Reson. 91*, 84−92.
Kleywegt, G. J., Vuister, G. W., Padilla, A., Knegtel, R. M. A, Boelens, R., & Kaptein, R. (1993) *J. Magn. Reson., Ser. B 102*, 166−176.
Knight, K. L., & Sauer, R. T. (1988) *Biochemistry 27*, 2088−2094.
Knight, K. L., & Sauer, R. T. (1989a) *Proc. Natl. Acad. Sci. U.S.A. 86*, 797−801.
Knight, K. L., & Sauer, R. T. (1989b) *J. Biol. Chem. 264*, 13706−13710.
Knight, K. L., & Sauer, R. T. (1992) *EMBO J. 11*, 215−223.
Knight, K. L., Bowie, J. U., Vershon, A. K., Kelley, R. D., & Sauer, R. T. (1989) *J. Biol. Chem. 264*, 3639−3642.
Kraulis, P. (1991) *J. Appl. Crystallogr. 24*, 946−950.
Marion, D., Kay, L. E., Sparks, S. W., Torchia, D. A., & Bax, A. (1989) *J. Am. Chem. Soc. 111*, 1515−1517.
Morris, A. L., MacArthur, M. W., Hutchinson, E. G., & Thornton, J. M. (1992) *Proteins: Struct., Funct., Genetics. 12*, 345−365.
Phillips, S. E. V. (1991) *Curr. Opin. Struct. Biol. 1*, 89−98.

Rafferty, J. B., Somers,W. S., Saint-Girons, I., & Phillips, S. E. V. (1989) *Nature 341*, 705−710.

Raumann, B. E., Rould, M. A., Pabo, C. O., & Sauer, R. T. (1994) *Nature 367*, 754−757.

Schulz, G. E., & Schirmer, R. H. (1979) *Principles of Protein Structure*, Springer-Verlag, New York, 98−101.

Somers, W. S., & Phillips, S. E. V. (1992) *Nature 259*, 387−393.

Susskind, M. M., & Youderian, P. (1983) in *Lambda II* (Hendrix, R. W., Roberts, J. W., Stahl, F. W., & Weisberg, R., Eds.) pp 347−366, Cold Spring Harbor Press, Cold Spring Harbor, NY.

Vershon, A. K., Youderian, P., Susskind, M. M., & Sauer, R. T. (1985) *J. Mol. Biol. 260*, 12124−12129.

Vershon, A. K., Liao, S.-M., McClure, W. R., & Sauer, R. T. (1987) *J. Mol. Biol. 195*, 311−322.

Wishart, D. S., Sykes, B. D., & Richards, F. M. (1991) *J. Mol. Biol. 222*, 311−333.

Wüthrich, K. (1986) *NMR of Proteins and Nucleic Acids*, Wiley, New York.

Youderian P., Vershon, A., Bouvier, S., Sauer R. T., & Susskind, M. M. (1983) *Cell, 35*, 777−783.

Zuiderweg, E. R. P., & Fesik, S. W. (1989) *Biochemistry 28*, 2387−2391.

Zuiderweg, E. R. P., McIntosh, L. P., Dahlquist, F. W., & Fesik, S. W. (1990) *J. Magn. Reson. 86*, 210−216.